Near-Field Low-WISL Unimodular Waveform Design for Terahertz Automotive Radar

Arian Eamaz[†,1], Farhang Yeganegi[†,2], Kumar Vijay Mishra[‡,3] and Mojtaba Soltanalian[†,4]
[†]University of Illinois, Chicago, IL 60607, USA
[‡]United States DEVCOM Army Research Laboratory, Adelphi, MD 20783 USA
email: {[1]aeamaz2, [2]fyegan2, [4]msol}@uic.edu, [3]kvm@ieee.org

***Abstract*—Conventional sensing applications rely on electromagnetic far-field channel models with plane wave propagation. However, recent ultra-short-range automotive radar applications at upper millimeter-wave or low terahertz (THz) frequencies envisage operation in the *near-field* region, where the wavefront is spherical. Unlike far-field, the near-field beampattern is dependent on both range and angle, thus requiring a different approach to waveform design. For the first time in the literature, we adopt the beampattern matching approach to design unimodular waveforms for THz automotive radars with low weighted integrated sidelobe levels (WISL). We formulate this problem as a unimodular bi-quadratic matrix program, and solve its constituent quadratic sub-problems using our cyclic power method-like iterations (CyPMLI) algorithm. Numerical experiments demonstrate that the CyPMLI approach yields the desired beampattern with low autocorrelation levels.**

***Index Terms*—Beampattern matching, near-field, spherical wave, THz automotive radar, unimodular waveform.**

I. Introduction

The shape of the propagating wavefront varies depending on the observation distance [1–3]. Accordingly, three distance regions have been identified [4]: near-field, Fresnel, and the far-field (Fraunhofer). The channel reciprocity phenomenon usually implies that these region categories may be effectively applied in a bidirectional manner, from both transmitter and receiver perspectives [5]. In the near-field, amplitude variations over the antenna aperture are noticeable [6]. In contrast, these variations are negligible in the Fresnel region, but phase variations still occur because of the signal's wavelength. In the far-field, both amplitude and phase variations are negligible; the amplitude (phase) depends only on the propagation distance (signal's incident angle) and the wavefront is approximated as locally planar. This leads to a linear propagation model via the Fourier theory.

Radar systems at lower sub-6 GHz frequencies rely on far-field plane-wave models as the antenna array is typically smaller than the operating wavelength [7]. However, with the advent of automotive radar applications at millimeter-wave and terahertz (THz) frequencies [8, 9] that employ electrically large arrays, the far-field assumption breaks down for short-range operation [10, 11]. At such ranges, the wavefront becomes spherical in the near-field [2–4], thereby requiring the use of Weyl's decomposition [12] of the spherical wave into several plane waves [7, 13]. This manifests itself in the array beampattern becoming a function of both angle and range [14].

Some far-field applications such as frequency diverse array (FDA) radars [15, 16] also exhibit range-dependent beampatterns, wherein linear frequency offsets in the carrier frequency across array elements results in a range-dependent beampattern without a spherical wavefront. Similar complex patterns are observed in quantum Rydberg arrays [17, 18]. In this paper, we focus on near-field THz-band automotive radars [19] that require consideration of range-dependent beampattern in system design [11, 20, 21]. THz-band automotive radars have attracted considerable research interest in recent years because of their potential for a near-optical resolution [11, 19]. While the literature indicates that a maximum range of 200 m is possible for THz automotive radars [22], most applications envisage their operation to be in the 10-20 m range [19].

Prior works on THz automotive radar waveform design have included distance-dependent channel models [19] and large arrays [9], but have ignored the near-field range-dependent beampattern shaping. Contrary to these works, we include near-field effects in our waveform design formulations. In particular, we focus on designing transmit signals with low correlation levels under the constraint of unimodularity [23, 24]. The upshot of this approach is the minimal peak-to-average-ratio (PAR) and avoiding gain non-linearities with low-cost amplifiers [25, 26]. Automotive radars often employ multiple-input multiple-output (MIMO) arrays to improve resolution without using many antennas [11]. In this case, the design problem requires obtaining a set of mutually (quasi-)orthogonal waveforms via minimization of the low integrated sidelobe level (ISL) or weighted ISL (WISL) [27–29] thereby leading to improved target extraction [30], resolution [31], and robustness [27].

We approach the near-field waveform design by adopting the beampattern matching approach [23, 32]. The WISL metric for beampattern matching leads to a *unimodular quartic matrix program* (UQMP). We then formulate the near-field waveform design problem as a *unimodular bi-quadratic matrix program* (UBQMP). Here, a quartic-to-bi-quadratic transformation splits the emerging UQMP into two quadratic matrix subproblems [33] that we solve using a low-complexity cyclic power method-like iterations (CyPMLI) algorithm [34, 35]. This is inspired by the power iteration method [24, 36, 37], which benefits from simple matrix-vector multiplications. Numerical experiments demonstrate that our proposed method achieves the desired beampattern while minimizing the WISL.

Throughout this paper, we use bold lowercase and bold uppercase letters for vectors and matrices, respectively. We represent a vector $\mathbf{x} \in \mathbb{C}^N$ in terms of its elements $\{x_i\}$ as $\mathbf{x} = [x_i]_{i=1}^N$. The mn-th element of the matrix $\mathbf{B}$ is $[\mathbf{B}]_{mn}$. The sets of complex and real numbers are $\mathbb{C}$ and $\mathbb{R}$, respectively; $(\cdot)^\top$, $(\cdot)^*$and $(\cdot)^\mathrm{H}$ are the vector/matrix transpose, conjugate and the Hermitian transpose, respectively. Trace of a matrix is denoted by $\mathrm{Tr}(.)$; the function $\mathrm{diag}(.)$ returns the diagonal elements of the input matrix. The Frobenius norm of a matrix $\mathbf{B} \in \mathbb{C}^{M \times N}$ is defined as $\|\mathbf{B}\|_\mathrm{F} = \sqrt{\sum_{r=1}^M \sum_{s=1}^N |b_{rs}|^2}$, where b_{rs} is the (r,s)-th entry of $\mathbf{B}$. The Hadamard (element-wise) and Kronecker products are $\odot$ and $\otimes$, respectively. The vectorized form of a matrix $\mathbf{B}$ is written as $\mathrm{vec}(\mathbf{B})$. The s-dimensional all-ones vector, all-zeros vector, and the identity matrix of size $s \times s$ are $\mathbf{1}_s$, $\mathbf{0}_N$, and $\mathbf{I}_s$, respectively. The real, imaginary, and angle/phase components of a complex number are $\mathrm{Re}(\cdot)$, $\mathrm{Im}(\cdot)$, and $\arg(\cdot)$, respectively.

II. System Model

Consider a MIMO radar with M linearly-spaced isotropic array elements, with the uniform inter-element spacing of d. The transmit antennas emit mutually orthogonal elements. The baseband signal transmitted by the m-th antenna is denoted by $x_m(t)$ with spectral support $\left[\frac{-B}{2}, \frac{B}{2}\right]$, and continuous-time Fourier transform (CTFT),

$$y_m(f) = \int_{-\infty}^{\infty} x_m(t) e^{-\mathrm{j}2\pi f t}\, dt, \quad f \in \left[-\frac{B}{2}, \frac{B}{2}\right]. \tag{1}$$

The baseband signal is then upconverted for transmission, in the form $s_m(t) = x_m(t) e^{\mathrm{j}2\pi f_c t}$, where f_c denotes the carrier frequency.

The utilization of an extremely small array aperture that is electrically large compared to the wavelength leads to near-field interactions with targets in close proximity. When the transmission range is shorter than the Fraunhofer distance $F = \frac{2D^2}{\lambda}$, where $D = (M-1)d$ is the array aperture and $d = \frac{\lambda}{2}$ with $\lambda = \frac{c_0}{f}$ being the wavelength, the wavefront is spherical. At the THz-band, the distance from the k-th target to the array origin, i.e., $p_k < F$ thereby requiring a near-field model [38].

The near-field steering vector $\mathbf{a}(\theta_k, p_k)$ corresponding to physical direction-of-arrival (DoA) θ_k and range p_k, is

$$\mathbf{a}(\theta_k, r_k) = \frac{1}{\sqrt{M}} \left[e^{-\mathrm{j}2\pi \frac{d}{\lambda} p_k^{(1)}}, \cdots, e^{-\mathrm{j}2\pi \frac{d}{\lambda} p_k^{(M)}}\right]^\top, \tag{2}$$

where $\theta_k = \sin\phi_k$, with $\phi_k \in \left[\frac{-\pi}{2}, \frac{\pi}{2}\right]$ and $p_k^{(m)}$ is the distance between the k-th target and the m-th antenna:

$$p_k^{(m)} = \sqrt{p_k^2 + 2(m-1)^2 d^2 - 2r_k(m-1)d\theta_k}. \tag{3}$$

According to the Fresnel approximation [1, 39], we can approximate (3) as

$$p_k^{(m)} \approx p_k - (m-1)d\theta_k + (m-1)^2 d^2 \zeta_k, \tag{4}$$

where $\zeta_k = \frac{1-\theta_k^2}{2p_k}$ is a function of both range and DoA. Substituting (4) into (2) gives

$$\mathbf{a}(\theta_k, p_k) \approx e^{-\mathrm{j}2\pi \frac{f_c}{c_0} p_k} \tilde{\mathbf{a}}(\theta_k, p_k), \tag{5}$$

where the m-th element of $\tilde{\mathbf{a}} \in \mathbb{C}^M$ is $[\tilde{\mathbf{a}}(\theta_k, p_k)]_m = e^{\mathrm{j}2\pi \frac{f_c}{c_0}\left((m-1)d\theta_k - (m-1)^2 d^2 \zeta_k\right)}$.

The (near-field) transmit signal at the location (θ_k, p_k) is

$$\begin{aligned} z_{\theta_k, p_k}(t) &= \sum_{m=1}^M s_m\left(t - \frac{dp_k^{(m)}}{c_0}\right), \\ &= \sum_{m=1}^M x_m\left(t - \frac{dp_k^{(m)}}{c_0}\right) e^{\mathrm{j}2\pi f_c \left(t - \frac{dp_k^{(m)}}{c_0}\right)}. \end{aligned} \tag{6}$$

Using the inverse CTFT of (1), we can rewrite $z_{\theta_k, p_k}(t)$ as

$$z_{\theta_k, p_k}(t) = \int_{-B/2}^{B/2} Y(\theta_k, p_k, f) e^{\mathrm{j}2\pi(f+f_c)t}\, df, \tag{7}$$

where $Y(\theta_k, p_k, f) = \sum_{m=1}^M y_m(f) e^{-\mathrm{j}2\pi(f+f_c)\frac{dp_k^{(m)}}{c_0}}$. As a result, the beampattern at location $\{\theta_k, p_k\}$ and frequency $f + f_c$ is $P(\theta_k, p_k, f) = |Y(\theta_k, p_k, f)|^2 = \left|\boldsymbol{\alpha}^\mathrm{H}(\theta_k, p_k, f)\mathbf{y}(f)\right|^2$, where $f \in \left[-\frac{B}{2}, \frac{B}{2}\right]$ and $\boldsymbol{\alpha}$ is obtained based on the approximated near-field steering vector (5):

$$\boldsymbol{\alpha}(\theta_k, p_k, f) = e^{-\mathrm{j}2\pi f} \mathbf{a}^\star(\theta_k, p_k), \tag{8}$$

and $\mathbf{y}(f) = \begin{bmatrix} y_1(f) & y_1(f) & \cdots & y_M(f) \end{bmatrix}^\top$. Sampling the signal $x_m(t)$ at the Nyquist interval $T_s = 1/B$, we obtain $x_m(n) = x_m(nT_s)$. The discrete Fourier transform (DFT) of $x_m(t)$ is

$$y_m(u) = \sum_{n=0}^{N-1} x_m(n) e^{-\mathrm{j}2\pi \frac{nu}{N}}, \; u \in \{0, 1, \cdots, N-1\}. \tag{9}$$

For ease of representation, we define the vector $\mathbf{y}_u = \begin{bmatrix} y_0(u) & y_1(u) & \cdots & y_{M-1}(u) \end{bmatrix}^\top$ which is comprised of the above DFT values.

We assume that the DoAs and ranges/delays $\{\theta_k, p_k\}$ are aligned to the grid points $\{\theta_{k_1}\}_{k_1=1}^{K_1}$ and $\{p_{k_2}\}_{k_2=1}^{K_2}$, where $\theta_{k_1} = \sin\phi_{k_1}$ with $\phi_{k_1} = \pi\left(\frac{k_1}{K_1} - \frac{1}{2}\right)$, $1 < k_1 < K_1$, and $p_{k_2} = \frac{k_2}{K_2}$, $1 < k_2 < K_2$. The grid size K_1 and K_2 are determined by the temporal and spatial sampling rates. The discretized $\boldsymbol{\alpha}$ is

$$\boldsymbol{\alpha}_{k_1, k_2, u} = \boldsymbol{\alpha}\left(\theta_{k_1}, p_{k_2}, \frac{u}{NT_s}\right). \tag{10}$$

The discretized beampattern becomes

$$P_{k_1, k_2, u} = \left|\boldsymbol{\alpha}_{k_1, k_2, u}^\mathrm{H} \mathbf{y}_u\right|^2. \tag{11}$$

Our goal is to design the waveform matrix $\mathbf{X} = [\mathbf{x}_1, \cdots, \mathbf{x}_M] \in \mathbb{C}^{M \times N}$ that will focus the beam in a desired direction.

III. Problem Formulation

A two-stage algorithm for far-field wideband MIMO waveform design was suggested in [40] based on the Gerchberg-Saxton algorithm [41]. The key idea here is to obtain a complex-valued waveform in the spectral domain such that $\mathbf{y}_u$ matches the magnitude of the desired beampattern as in (11). Related techniques also include phase-retrieval-based waveform design [42, 43]. We address the near-field version of this problem without resorting to phase retrieval methods.

A. Beampattern Matching Formulation

Denote the desired beampattern by $\left\{\widehat{P}_{k_1,k_2,u}\right\}$. The set of complex unimodular sequences is identified as

$$\Omega^N = \left\{\mathbf{s} \in \mathbb{C}^N | s(l) = e^{\mathrm{j}\omega_l}, \omega_l \in [0, 2\pi),\ 0 \le l \le N-1\right\}. \tag{12}$$

The beampattern matching optimization problem is [44],

$$\underset{\mathbf{x}_m \in \Omega^N}{\text{minimize}} \sum_{k_1=1}^{K_1} \sum_{k_2=1}^{K_2} \sum_{u=0}^{N-1} \left[\widehat{P}_{k_1,k_2,u} - \left|\boldsymbol{\alpha}^{\mathrm{H}}_{k_1,k_2,u} \mathbf{y}_u\right|^2\right]^2. \tag{13}$$

To directly tackle (13) with respect to $\mathbf{X}$, we write $\mathbf{y}_u$ as $\mathbf{y}_u = \mathbf{X}^\top \mathbf{f}_u$, where $\mathbf{f}_u = \left[\begin{array}{cccc} 1 & e^{-\mathrm{j}2\pi\frac{u}{N}} & \dots & e^{-\mathrm{j}2\pi\frac{(N-1)u}{N}} \end{array}\right]^\top$ is the DFT vector. Then, (13) becomes

$$\underset{\mathbf{x}_m \in \Omega^N}{\text{minimize}} \sum_{k_1=1}^{K_1} \sum_{k_2=1}^{K_2} \sum_{u=0}^{N-1} \left[\widehat{P}_{k_1,k_2,u} - \left|\boldsymbol{\alpha}^{\mathrm{H}}_{k_1,k_2,u} \mathbf{X}^\top \mathbf{f}_u\right|^2\right]^2, \tag{14}$$

Expanding the objective $\mathcal{P} = \left[\widehat{P}_{k_1,k_2,u} - \left|\boldsymbol{\alpha}^{\mathrm{H}}_{k_1,k_2,u} \mathbf{X}^\top \mathbf{f}_u\right|^2\right]^2$, we obtain a quartic formulation is

$$\begin{aligned}\mathcal{P} = {} & \mathbf{f}_u^{\mathrm{H}} \mathbf{X}^\star \boldsymbol{\alpha}_{k_1,k_2,u} \boldsymbol{\alpha}^{\mathrm{H}}_{k_1,k_2,u} \mathbf{X}^\top \mathbf{f}_u \mathbf{f}_u^{\mathrm{H}} \mathbf{X}^\star \boldsymbol{\alpha}_{k_1,k_2,u} \boldsymbol{\alpha}^{\mathrm{H}}_{k_1,k_2,u} \mathbf{X}^\top \mathbf{f}_u - \\ & 2\widehat{P}_{k_1,k_2,u} \mathbf{f}_u^{\mathrm{H}} \mathbf{X}^\star \boldsymbol{\alpha}_{k_1,k_2,u} \boldsymbol{\alpha}^{\mathrm{H}}_{k_1,k_2,u} \mathbf{X}^\top \mathbf{f}_u + \widehat{P}^2{}_{k_1,k_2,u}.\end{aligned} \tag{15}$$

Note that $\boldsymbol{\alpha}^{\mathrm{H}}_{k_1,k_2,u} \mathbf{X}^\top \mathbf{f}_u$ is scalar. Hence,

$$\begin{aligned}&\mathbf{f}_u^{\mathrm{H}} \mathbf{X}^\star \boldsymbol{\alpha}_{k_1,k_2,u} \boldsymbol{\alpha}^{\mathrm{H}}_{k_1,k_2,u} \mathbf{X}^\top \mathbf{f}_u = \\ &\qquad \mathrm{vec}^\top\left(\mathbf{f}_u^{\mathrm{H}} \mathbf{X}^\star \boldsymbol{\alpha}_{k_1,k_2,u}\right) \mathrm{vec}\left(\boldsymbol{\alpha}^{\mathrm{H}}_{k_1,k_2,u} \mathbf{X}^\top \mathbf{f}_u\right),\end{aligned} \tag{16}$$

where according to the identities of vectorization operator [36], we have $\mathrm{vec}\left(\mathbf{f}_u^{\mathrm{H}} \mathbf{X}^\star \boldsymbol{\alpha}_{k_1,k_2,u}\right) = \mathbf{f}_u^{\mathrm{H}} \mathrm{vec}\left(\mathbf{X}^\star \boldsymbol{\alpha}_{k_1,k_2,u}\right) = \mathbf{f}_u^{\mathrm{H}} \left(\boldsymbol{\alpha}^\top_{k_1,k_2,u} \otimes \mathbf{I}_N\right) \mathrm{vec}\left(\mathbf{X}^\star\right)$, and $\mathrm{vec}\left(\boldsymbol{\alpha}^{\mathrm{H}}_{k_1,k_2,u} \mathbf{X}^\top \mathbf{f}_u\right) = \boldsymbol{\alpha}^{\mathrm{H}}_{k_1,k_2,u} \mathrm{vec}\left(\mathbf{X}^\top \mathbf{f}_u\right) = \boldsymbol{\alpha}^{\mathrm{H}}_{k_1,k_2,u} \left(\mathbf{f}_u^\top \otimes \mathbf{I}_M\right) \mathrm{vec}\left(\mathbf{X}^\top\right)$. Consequently,

$$\begin{aligned}&\mathbf{f}_u^{\mathrm{H}} \mathbf{X}^\star \boldsymbol{\alpha}_{k_1,k_2,u} \boldsymbol{\alpha}^{\mathrm{H}}_{k_1,k_2,u} \mathbf{X}^\top \mathbf{f}_u = \\ &\mathrm{vec}^\top\left(\mathbf{X}^\star\right) \left(\boldsymbol{\alpha}_{k_1,k_2,u} \otimes \mathbf{I}_N\right) \mathbf{f}_u^\star \boldsymbol{\alpha}^{\mathrm{H}}_{k_1,k_2,u} \left(\mathbf{f}_u^\top \otimes \mathbf{I}_M\right) \mathrm{vec}\left(\mathbf{X}^\top\right)\end{aligned} \tag{17}$$

Using the commutation matrix $\mathbf{P}$, i.e., $\mathrm{vec}\left(\mathbf{X}^\top\right) = \mathbf{P}\,\mathrm{vec}\left(\mathbf{X}\right)$ and the fact that $\mathrm{vec}^\top\left(\mathbf{X}^\star\right) = \mathrm{vec}^{\mathrm{H}}\left(\mathbf{X}\right)$, (17) becomes $\mathbf{f}_u^{\mathrm{H}} \mathbf{X}^\star \boldsymbol{\alpha}_{k_1,k_2,u} \boldsymbol{\alpha}^{\mathrm{H}}_{k_1,k_2,u} \mathbf{X}^\top \mathbf{f}_u = \mathrm{vec}^{\mathrm{H}}\left(\mathbf{X}\right) \mathbf{G}\,\mathrm{vec}\left(\mathbf{X}\right)$, where $\mathbf{G} = \left(\boldsymbol{\alpha}_{k_1,k_2,u} \otimes \mathbf{I}_N\right) \mathbf{f}_u^\star \boldsymbol{\alpha}^{\mathrm{H}}_{k_1,k_2,u} \left(\mathbf{f}_u^\top \otimes \mathbf{I}_M\right) \mathbf{P}$. Thus, the objective of (14) is reformulated to

$$\mathcal{P} = \mathrm{vec}^{\mathrm{H}}\left(\mathbf{X}\right) \left(\mathcal{G}\left(\mathbf{X}\right) - 2\widehat{P}_{k_1,k_2,u} \mathbf{G}\right) \mathrm{vec}\left(\mathbf{X}\right) + \widehat{P}^2{}_{k_1,k_2,u} \tag{18}$$

where $\mathcal{G}\left(\mathbf{X}\right) = \mathbf{G}\,\mathrm{vec}\left(\mathbf{X}\right) \mathrm{vec}^{\mathrm{H}}\left(\mathbf{X}\right) \mathbf{G}$. The beampattern matching problem is now formulated as the following quartic matrix program (QMP):

$$\underset{\mathbf{x}_m \in \Omega^N}{\text{minimize}}\ \mathrm{vec}^{\mathrm{H}}\left(\mathbf{X}\right) \widehat{\mathbf{G}}\left(\mathbf{X}\right) \mathrm{vec}\left(\mathbf{X}\right), \tag{19}$$

with $\widehat{\mathbf{G}}\left(\mathbf{X}\right) = \sum_{k_1=1}^{K_1} \sum_{k_2=1}^{K_2} \sum_{u=0}^{N-1} \left[\mathcal{G}\left(\mathbf{X}\right) - 2\widehat{P}_{k_1,k_2,u} \mathbf{G}\right]$.

B. WISL Criterion for Unimodular Waveform Design

Consider a collection of M unimodular waveforms, each with a code length of N. The cross-correlation between the m-th and m'-th waveforms of sequences is $r_{mm'}(k) = \sum_{l=0}^{N-k-1} x_m(l) x^\star_{m'}(l+k) = r^\star_{mm'}(-k)$ [44]. Denote $\tau_{mmk} = \left|r_{mm}(k)\right|^2$ and $\eta_{mm'k} = \left|r_{mm'}(k)\right|^2$. The WISL criterion of waveform $\mathbf{X}$ is [44]

$$\mathcal{W} = \sum_{m=1}^{M} \sum_{\substack{k=-N+1 \\ k \neq 0}}^{N-1} \omega_k^2 \eta_{mmk} + \sum_{m=1}^{M} \sum_{m'=1 m' \neq m}^{M} \sum_{k=-N+1}^{N-1} \omega_k^2 \eta_{mm'k}, \tag{20}$$

where $\{\omega_k\}_{k=1}^{N}$ are weights.

The unimodular waveform with good correlation properties is obtained by solving the following optimization problem:

$$\underset{\mathbf{x}_m \in \Omega^N}{\text{minimize}}\ \mathcal{W}. \tag{21}$$

Following [45], this WISL minimization boils down to

$$\underset{\mathbf{x}_m \in \Omega^N}{\text{minimize}}\ \sum_{k=1}^{2N} \left\|\mathbf{X}^{\mathrm{H}}\left(\left(\boldsymbol{\beta}_k \boldsymbol{\beta}_k^{\mathrm{H}}\right) \odot \boldsymbol{\Gamma}\right) \mathbf{X}\right\|_{\mathrm{F}}^2, \tag{22}$$

where $\boldsymbol{\Gamma} \in \mathbb{R}^{N \times N}$ is a Toeplitz matrix whose upper and lower triangular parts are constructed by the weights $\{\omega_k\}_{k=0}^{N-1}$ and $\{\omega_{-k}\}_{k=1}^{N-1}$, respectively, i.e., $\boldsymbol{\Gamma} \triangleq \begin{bmatrix} \omega_0 & \omega_1 & \cdots & \omega_{N-1} \\ \omega_{-1} & \omega_0 & \ddots & \vdots \\ \vdots & \ddots & \ddots & \omega_1 \\ \omega_{-N+1} & \cdots & \omega_{-1} & \omega_0 \end{bmatrix}$ and $\boldsymbol{\beta}_k = \left[\begin{array}{cccc} 1 & e^{\mathrm{j}2\pi\frac{(k-1)}{2N}} & \dots & e^{\mathrm{j}2\pi\frac{(N-1)(k-1)}{2N}} \end{array}\right]^\top$.

C. Low-WISL Waveform Design via UQMP

To tackle the WISL minimization problem with our proposed algorithm, which is a variant of the power iteration method, we reshape the objective to bring it to the standard form with $\mathbf{s}^{\mathrm{H}}\mathbf{R}\mathbf{s}$, $\mathbf{s} \in \mathbb{C}^N$, $\mathbf{R} \in \mathbb{R}^{N \times N}$. To do so, we substitute $\mathbf{J}_k = \left(\boldsymbol{\beta}_k \boldsymbol{\beta}_k^{\mathrm{H}}\right) \odot \boldsymbol{\Gamma}$ in the objective as

$$\left\|\mathbf{X}^{\mathrm{H}} \mathbf{J}_k \mathbf{X}\right\|_{\mathrm{F}}^2 = \mathrm{vec}^{\mathrm{H}}\left(\mathbf{X}\right) \left(\mathbf{I}_M \otimes \mathbf{J}_k^{\mathrm{H}} \mathbf{X} \mathbf{X}^{\mathrm{H}} \mathbf{J}_k\right) \mathrm{vec}\left(\mathbf{X}\right). \tag{23}$$

Define $\mathcal{J}\left(\mathbf{X}\right) = \sum_{k=1}^{2N} \left(\mathbf{I}_M \otimes \mathbf{J}_k^{\mathrm{H}} \mathbf{X} \mathbf{X}^{\mathrm{H}} \mathbf{J}_k\right) = \mathbf{I}_M \otimes \left(\sum_{k=1}^{2N} \mathbf{J}_k^{\mathrm{H}} \mathbf{X} \mathbf{X}^{\mathrm{H}} \mathbf{J}_k\right)$. The WISL minimization problem is now recast as a UQMP as follows:

$$\underset{\mathbf{x}_m \in \Omega^N}{\text{minimize}}\ \mathrm{vec}^{\mathrm{H}}\left(\mathbf{X}\right) \mathcal{J}\left(\mathbf{X}\right) \mathrm{vec}\left(\mathbf{X}\right). \tag{24}$$

Now, both (19) and (24) share the same form and can be optimized together in a single optimization problem. Hence, we consider the following optimization problem that designs a unimodular waveform with a low-WISL while incorporating beampattern matching requirements:

$$\underset{\mathbf{x}_m \in \Omega^N}{\text{minimize}}\ \gamma\mathcal{P} + (1-\gamma)\mathcal{W} \tag{25}$$

where $0 \le \gamma \le 1$ is the Lagrangian multiplier. The resulting UQMP is

$$\underset{\mathbf{x}_m \in \Omega^N}{\text{minimize}}\ \mathrm{vec}^{\mathrm{H}}\left(\mathbf{X}\right) \left(\gamma\widehat{\mathbf{G}}\left(\mathbf{X}\right) + (1-\gamma)\mathcal{J}\left(\mathbf{X}\right)\right) \mathrm{vec}\left(\mathbf{X}\right). \tag{26}$$

IV. Proposed Algorithm

Our approach to solve the low-WISL waveform design problem (26) is to cast it as a UBQMP and then tackle it using the CyPMLI algorithm. Define $\mathbf{R}\left(\mathbf{X}\right) = \left(\gamma\widehat{\mathbf{G}}\left(\mathbf{X}\right) + (1-\gamma)\mathcal{J}\left(\mathbf{X}\right)\right)$. To transform (26) into two quadratic optimization subproblems, we define two variables $\text{vec}(\mathbf{X}_1)$ and $\text{vec}(\mathbf{X}_2)$. It is also interesting to observe that if either $\mathbf{X}_1$ or $\mathbf{X}_2$ are fixed, solving (26) with respect to the other variable can be done via a unimodular quadratic programming (UQP) formulation [34, 46]:

$$\underset{\text{vec}(\mathbf{X}_j)\in\Omega^{NM}}{\text{minimize}} \quad \text{vec}^{\text{H}}(\mathbf{X}_j)\,\mathbf{R}(\mathbf{X}_i)\,\text{vec}(\mathbf{X}_j), \quad i \neq j \in \{1,2\}. \tag{27}$$

To ensure the convergence of $\mathbf{X}_1$ and $\mathbf{X}_2$ to the same waveform matrix, a connection needs to be established between them in the objective. By adding the Frobenius norm error between $\mathbf{X}_1$ and $\mathbf{X}_2$ as a *penalty* with the Lagrangian multiplier to (27), we have the following *regularized Lagrangian* problem:

$$\underset{\text{vec}(\mathbf{X}_j)\in\Omega^{NM}}{\text{minimize}} \quad \text{vec}^{\text{H}}(\mathbf{X}_j)\,\mathbf{R}(\mathbf{X}_i)\,\text{vec}(\mathbf{X}_j) + \rho\,\|\mathbf{X}_i - \mathbf{X}_j\|_{\text{F}}^2, \tag{28}$$

where ρ is the Lagrangian multiplier. The penalty $\|\mathbf{X}_i - \mathbf{X}_j\|_{\text{F}}^2$ is also a quadratic function with respect to $\mathbf{X}_j$. Consequently, the UBQMP formulation for (26) is given by below:

$$\underset{\text{vec}(\mathbf{X}_j)\in\Omega^{NM}}{\text{minimize}} \begin{pmatrix}\text{vec}(\mathbf{X}_j)\\ 1\end{pmatrix}^{\text{H}} \underbrace{\begin{pmatrix}\mathbf{R}(\mathbf{X}_i) & -\rho\,\text{vec}(\mathbf{X}_i)\\ -\rho\,\text{vec}^{\text{H}}(\mathbf{X}_i) & 2\rho NM\end{pmatrix}}_{\breve{\mathbf{R}}(\mathbf{X}_i)} \begin{pmatrix}\text{vec}(\mathbf{X}_j)\\ 1\end{pmatrix}, \tag{29}$$

To employ CyPMLI, we need to transform the problem to a maximization problem using the *diagonal loading process*. Denote the maximum eigenvalue of $\breve{\mathbf{R}}(\mathbf{X}_i)$ by λ_m, where $\lambda_m\mathbf{I} \succeq \breve{\mathbf{R}}(\mathbf{X}_i)$. Thus, $\widehat{\mathbf{R}}(\mathbf{X}_i) = \lambda_m\mathbf{I} - \mathbf{R}(\mathbf{X}_i)$ is positive definite [34]. Note that a diagonal loading with $\lambda_m\mathbf{I}$ has no effect on the solution of (29) due to the fact that $\|\mathbf{X}\|_{\text{F}}^2 = NM$ and $\text{vec}^{\text{H}}(\mathbf{X}_j)\,\widehat{\mathbf{R}}(\mathbf{X}_i)\,\text{vec}(\mathbf{X}_j) = \lambda_m NM - \text{vec}^{\text{H}}(\mathbf{X}_j)\,\mathbf{R}(\mathbf{X}_i)\,\text{vec}(\mathbf{X}_j)$. Therefore, we have the following equivalent form of (29):

$$\underset{\text{vec}(\mathbf{X}_j)\in\Omega^{NM}}{\text{maximize}} \begin{pmatrix}\text{vec}(\mathbf{X}_j)\\ 1\end{pmatrix}^{\text{H}} \underbrace{\begin{pmatrix}\widehat{\mathbf{R}}(\mathbf{X}_i) & \rho\,\text{vec}(\mathbf{X}_i)\\ \rho\,\text{vec}^{\text{H}}(\mathbf{X}_i) & \widehat{\rho}\end{pmatrix}}_{\mathcal{R}(\mathbf{X}_i)} \begin{pmatrix}\text{vec}(\mathbf{X}_j)\\ 1\end{pmatrix}, \tag{30}$$

where $\widehat{\rho} = \lambda_m - 2\rho NM$. The desired matrix $\mathbf{X}_j$ of (30) is readily evaluated by PMLI at convergence using the iterations $\mathbf{v}^{(t+1)} = e^{\text{j}\arg\left(\mathcal{R}(\mathbf{X}_i)\mathbf{v}^{(t)}\right)}$ [34], where $\mathbf{v} = \left(\text{vec}^{\top}(\mathbf{X}_j) \;\; 1\right)^{\top}$. This update process can be simplified as

$$\text{vec}\left(\mathbf{X}_j^{(t+1)}\right) = e^{\text{j}\arg\left(\widehat{\mathbf{R}}\left(\mathbf{X}_i^{(t)}\right)\text{vec}\left(\mathbf{X}_j^{(t)}\right) + \rho\,\text{vec}\left(\mathbf{X}_i^{(t)}\right)\right)}. \tag{31}$$

Such power method-like iterations are already shown to be convergent in terms of both the objective and the signal [24, 35], implying that $\mathbf{X}_1$ and $\mathbf{X}_2$ will be converging to each other as well.

V. Numerical Experiments

We numerically evaluated the efficacy of our approach. We used the following settings for our experiments: the number of array elements is $M = 4$, the carrier frequency of the transmitted signal is $f_c = 1$ GHz, the bandwidth $B = 200$ MHz, and the number of symbols is $N = 64$. The inter-element spacing is $d = c_0/(2(f_c + B/2))$ (half wavelength of the highest in-band frequency) to avoid grating lobes. The DoA (normalized range) domain set of $-\frac{\pi}{2} \leq \phi \leq \frac{\pi}{2}$ $(0 < p \leq 1)$ was discretized with $K_1 = 20$ and $K_2 = 10$ grid points.

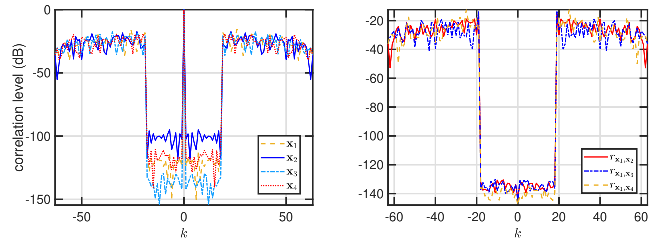

(a) (b)

Figure 1. (a) The correlation level of the designed waveform with sequence length $N = 64$ for antenna array with $M = 4$ elements. (b) The cross-correlation between $\mathbf{x}_1$ and other sequences in the designed waveform; i.e. $\mathbf{x}_2$, $\mathbf{x}_3$ and $\mathbf{x}_4$ with the same values of N and M as in (a). Note that the sequences have been designed to suppress the correlation levels at lags from $k = -20$ to $k = 20$.

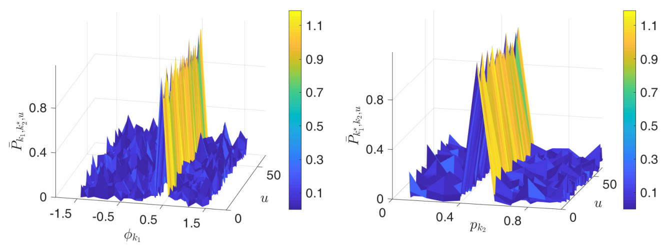

(a) (b)

Figure 2. The obtained near-field beampattern with respect to (a) $-\frac{\pi}{2} \leq \phi_{k_1} \leq \frac{\pi}{2}$ and u for fixed $k_1 = k_1^{\star}$, and (b) $0 < p_{k_2} \leq 1$ and u for fixed $k_2 = k_2^{\star}$. In all cases, we have $N = 64$ and $M = 4$.

The CyPMLI parameters are set as $\rho = 2$ and $\gamma = 0.5$. We updated the value of λ_m according to [34, Theorem 1]. Fig. 1a shows that the resulting waveform achieves a satisfactory correlation level. Further, the designed sequences exhibit a good cross-correlation property with each other (Fig. 1b). For numerical evaluation, we consider the desired beampattern to be 1 at the indices $k_1^{\star}$ and $k_2^{\star}$ and 0 elsewhere for all u. Fig. 2a displays the (near-field) beampattern obtained for the angular span of $-\frac{\pi}{2} \leq \phi_{k_1} \leq \frac{\pi}{2}$ and discrete frequency u with fixed $k_1 = k_1^{\star}$. On the other hand, Fig. 2b shows the beampattern as a function of range $0 < p_{k_2} \leq 1$ and u with fixed $k_2 = k_2^{\star}$. Moreover, CyPMLI maintains good input correlation properties as shown in Fig. 1 while obtaining the desired beampattern with a small negligible error.

VI. Summary

THz automotive radars are expected to provide near-optical resolution approaching lidars. For the ultrashort range operation, near-field propagation needs to be considered in the waveform design for these systems. We proposed CyPMLI approach to obtain low-WISL unimodular waveforms and realize the range-dependent beampattern in near-field.

Acknowledgement

A.E., F.Y., and M.S. acknowledge partial support via National Science Foundation Grant ECCS-1809225.

References

[1] M. Gustafsson and S. Nordebo, "Characterization of MIMO antennas using spherical vector waves," *IEEE Transactions on Antennas and Propagation*, vol. 54, no. 9, pp. 2679–2682, 2006.

[2] A. Glazunov, M. Gustafsson, A. Molisch, F. Tufvesson, and G. Kristensson, "Spherical vector wave expansion of Gaussian electromagnetic fields for antenna-channel interaction analysis," *IEEE Transactions on Antennas and Propagation*, vol. 57, no. 7, pp. 2055–2067, 2009.

[3] A. Glazunov, M. Gustafsson, A. Molisch, and F. Tufvesson, "Physical modelling of multiple-input multiple-output antennas and channels by means of the spherical vector wave expansion," *IET Microwaves, Antennas & Propagation*, vol. 4, no. 6, pp. 778–791, 2010.

[4] E. Björnson, Ö. Demir, and L. Sanguinetti, "A primer on near-field beamforming for arrays and reconfigurable intelligent surfaces," in *Asilomar Conference on Signals, Systems, and Computers*, 2021, pp. 105–112.

[5] K. Selvan and R. Janaswamy, "Fraunhofer and Fresnel distances: Unified derivation for aperture antennas." *IEEE Antennas and Propagation Magazine*, vol. 59, no. 4, pp. 12–15, 2017.

[6] B. Friedlander, "Localization of signals in the near-field of an antenna array," *IEEE Transactions on Signal Processing*, vol. 67, no. 15, pp. 3885–3893, 2019.

[7] M. E. Yanik, D. Wang, and M. Torlak, "Development and demonstration of MIMO-SAR mmWave imaging testbeds," *IEEE Access*, vol. 8, pp. 126 019–126 038, 2020.

[8] A. M. Elbir, K. V. Mishra, S. Chatzinotas, and M. Bennis, "Terahertz-band integrated sensing and communications: Challenges and opportunities," *arXiv preprint arXiv:2208.01235*, 2022.

[9] A. M. Elbir, K. V. Mishra, and S. Chatzinotas, "Terahertz-band joint ultra-massive MIMO radar-communications: Model-based and model-free hybrid beamforming," *IEEE Journal of Selected Topics in Signal Process.*, vol. 15, no. 6, pp. 1468–1483, 2021.

[10] H. Sarieddeen, M. Alouini, and T. Al-Naffouri, "An overview of signal processing techniques for terahertz communications," *Proceedings of the IEEE*, vol. 109, no. 10, pp. 1628–1665, 2021.

[11] K. V. Mishra, I. Bilik, J. Tabrikian, and A. P. Petropulu, "Signal processing for terahertz-band automotive radars: Exploring the next frontier," *arXiv preprint*, 2023.

[12] H. Weyl, "Ausbreitung elektromagnetischer wellen über einem ebenen leiter," *Annalen der Physik*, vol. 365, no. 21, pp. 481–500, 1919.

[13] Y. Meng, C. Lin, A. Qing, and N. K. Nikolova, "Accelerated holographic imaging with range stacking for linear frequency modulation radar," *IEEE Transactions on Microwave Theory and Techniques*, vol. 70, no. 3, pp. 1630–1638, 2021.

[14] A. Elbir, M. K. V., and S. Chatzinotas, "NBA-OMP: Near-field beam-split-aware orthogonal matching pursuit for wideband THz channel estimation," in *IEEE International Conference on Acoustics, Speech and Signal Processing*, 2023, in press.

[15] W. Lv, K. V. Mishra, and S. Chen, "Co-pulsing FDA radar," *IEEE Transactions on Aerospace and Electronic Systems*, 2022, in press.

[16] ——, "Clutter suppression via space-time-range processing in co-pulsing FDA radar," in *Asilomar Conference on Signals, Systems, and Computers*, 2022, in press.

[17] P. Vouras, K. V. Mishra, A. Artusio-Glimpse, S. Pinilla, A. Xenaki, D. W. Griffith, and K. Egiazarian, "An overview of advances in signal processing techniques for classical and quantum wideband synthetic apertures," *IEEE Journal of Selected Topics in Signal Processing*, 2023, in press.

[18] P. Vouras, K. V. Mishra, and A. Artusio-Glimpse, "Phase retrieval for Rydberg quantum arrays," in *IEEE International Conference on Acoustics, Speech and Signal Processing*, 2023, in press.

[19] S. Bhattacharjee, K. V. Mishra, R. Annavajjala, and C. R. Murthy, "Multi-carrier wideband OCDM-based THz automotive radar," in *IEEE International Conference on Acoustics, Speech and Signal Processing*, 2023, in press.

[20] A. M. Elbir, K. V. Mishra, S. A. Vorobyov, and W. Heath Robert, Jr., "Twenty-five years of advances in beamforming: From convex and nonconvex optimization to learning techniques," *arXiv preprint arXiv:2211.02165*, 2022.

[21] A. M. Elbir, K. V. Mishra, A. Abdallah, A. Celik, and A. M. Eltawil, "Spatial path index modulation in mmWave/THz-band integrated sensing and communications," *arXiv preprint*, 2023.

[22] F. Norouzian, E. Marchetti, M. Gashinova, E. Hoare, C. Constantinou, P. Gardner, and M. Cherniakov, "Rain attenuation at millimeter wave and low-THz frequencies," *IEEE Transactions on Antennas and Propagation*, vol. 68, no. 1, pp. 421–431, 2019.

[23] P. Stoica, H. He, and J. Li, "New algorithms for designing unimodular sequences with good correlation properties," *IEEE Transactions on Signal Processing*, vol. 57, no. 4, pp. 1415–1425, 2009.

[24] M. Soltanalian and P. Stoica, "Designing unimodular codes via quadratic optimization," *IEEE Transactions on Signal Processing*, vol. 62, no. 5, pp. 1221–1234, 2014.

[25] Z. Cheng, Z. He, S. Zhang, and J. Li, "Constant modulus waveform design for MIMO radar transmit beampattern," *IEEE Transactions on Signal Processing*, vol. 65, no. 18, pp. 4912–4923, 2017.

[26] A. Aubry, A. De Maio, and M. M. Naghsh, "Optimizing radar waveform and Doppler filter bank via generalized fractional programming," *IEEE Journal of Selected Topics in Signal Processing*, vol. 9, no. 8, pp. 1387–1399, 2015.

[27] H. He, J. Li, and P. Stoica, *Waveform design for active sensing systems: a computational approach*. Cambridge University Press, 2012.

[28] Y. Li, C. Shi, and R. Tao, "Unimodular waveform design with low correlation levels: A fast algorithm development to support large-scale code lengths," in *IEEE International Conference on Acoustics, Speech and Signal Processing*, 2022, pp. 4983–4987.

[29] M. Alaee-Kerahroodi, M. Soltanalian, P. Babu, and M. B. Shankar, *Signal Design for Modern Radar Systems*. Artech House, 2022.

[30] A. Aubry, A. De Maio, Y. Huang, and M. Piezzo, "Robust design of radar Doppler filters," *IEEE Transactions on Signal Processing*, vol. 64, no. 22, pp. 5848–5860, 2016.

[31] Y. Li, S. Vorobyov, and V. Koivunen, "Ambiguity function of the transmit beamspace-based MIMO radar," *IEEE Transactions on Signal Processing*, vol. 63, no. 17, pp. 4445–4457, 2015.

[32] M. Soltanalian, H. Hu, and P. Stoica, "Single-stage transmit beamforming design for mimo radar," *Signal Processing*, vol. 102, pp. 132–138, 2014.

[33] A. Beck, "Quadratic matrix programming," *SIAM Journal on Optimization*, vol. 17, no. 4, pp. 1224–1238, 2007.

[34] A. Eamaz, F. Yeganegi, and M. Soltanalian, "CyPMLI: WISL-minimized unimodular sequence design via power method-like iterations," in *ICASSP 2023-2023 IEEE International Conference on Acoustics, Speech and Signal Processing (ICASSP)*. IEEE, 2023, pp. 1–5.

[35] ——, "MaRLI: Attack on the discrete-phase WISL minimization problem," *arXiv preprint arXiv*, 2023.

[36] C. Van Loan and G. Golub, *Matrix computations*. The Johns Hopkins University Press, 1996.

[37] M. Soltanalian, B. Tang, J. Li, and P. Stoica, "Joint design of the receive filter and transmit sequence for active sensing," *IEEE Signal Processing Letters*, vol. 20, no. 5, pp. 423–426, 2013.

[38] A. Elbir, W. Shi, A. Papazafeiropoulos, P. Kourtessis, and S. Chatzinotas, "Terahertz-band channel and beam split estimation via array perturbation model," *arXiv preprint arXiv:2208.03683*, 2022.

[39] M. Cui, L. Dai, Z. Wang, S. Zhou, and N. Ge, "Near-field rainbow: Wideband beam training for XL-MIMO," *IEEE Transactions on Wireless Communications*, 2022, in press.

[40] J. Li, Y. Xie, P. Stoica, X. Zheng, and J. Ward, "Beampattern synthesis via a matrix approach for signal power estimation," *IEEE Transactions on Signal Processing*, vol. 55, no. 12, pp. 5643–5657, 2007.

[41] R. Gerchberg, "A practical algorithm for the determination of plane from image and diffraction pictures," *Optik*, vol. 35, no. 2, pp. 237–246, 1972.

[42] S. Pinilla, K. V. Mishra, B. M. Sadler, and H. Arguello, "Phase retrieval for radar waveform design," *arXiv preprint arXiv:2201.11384*, 2022.

[43] S. Pinilla, K. V. Mishra, and B. Sadler, "WaveMax: FrFT-based convex phase retrieval for radar waveform design," in *IEEE International Symposium on Information Theory*, 2021, pp. 2387–2392.

[44] H. He, P. Stoica, and J. Li, "Designing unimodular sequence sets with good correlations—including an application to MIMO radar," *IEEE Transactions on Signal Processing*, vol. 57, no. 11, pp. 4391–4405, 2009.

[45] Y. Li and S. Vorobyov, "Fast algorithms for designing unimodular waveform(s) with good correlation properties," *IEEE Transactions on Signal Processing*, vol. 66, no. 5, pp. 1197–1212, 2017.

[46] Z. Esmaeilbeig, A. Eamaz, K. V. Mishra, and M. Soltanalian, "Joint waveform and passive beamformer design in multi-IRS-aided radar," in *ICASSP 2023-2023 IEEE International Conference on Acoustics, Speech and Signal Processing (ICASSP)*. IEEE, 2023, pp. 1–5.